Hypoxic Tumour Cell-derived Exosomal miR-340-5p Promotes Radioresistance of Oesophageal Squamous Cell Carcinoma via KLF10

Fangyu Chen
The First Affiliated Hospital of Nanjing Medical University
Bing Xu
The First Affiliated Hospital of Nanjing Medical University
Jie Li
The First Affiliated Hospital of Nanjing Medical University
Xi Yang
Fudan University Shanghai Cancer Center
Junjie Gu
The First Affiliated Hospital of Nanjing Medical University
Xijuan Yao
The First Affiliated Hospital of Nanjing Medical University
Xinchen Sun (sunxinchen@njmu.edu.cn)
Department of Radiation Oncology, The First Affiliated Hospital of Nanjing Medical University, Nanjing, China.

Research

Keywords: hypoxia, extracellular vesicles, miRNA, oesophageal cancer, radiotherapy

Posted Date: September 15th, 2020

DOI: https://doi.org/10.21203/rs.3.rs-75570/v1

Version of Record: A version of this preprint was published on January 23rd, 2021. See the published version at https://doi.org/10.1186/s13046-021-01834-9.

Abstract

Background: Radiotherapy resistance is a major obstacle in the treatment of oesophageal squamous cell carcinoma (OSCC). Hypoxia is a critical cause of radioresistance. However, the communications between hypoxic cells and aerobic cells via exosomes during radiation resistance remain unclear.

Methods: We previously detected miR-340-5p is highly expressed in hypoxic OSCC exosomes by RNA-seq. The effects and mechanisms of hypoxic EVs and miR-340-5p on radiosensitivity were evaluated by qPCR, western blot IHC, flow cytometry, TUNEL assay, etc. Tumour xenografts and clinical samples were used for evaluating radiosensitivity and dissecting underlying mechanisms.

Results: Hypoxic exosomes can alleviate radiation induced apoptosis and accelerate DNA damage repair. miR-340-5p is highly expressed in hypoxic exosomes and causes radioresistance. Knockdown miR-340-5p in hypoxic EVs reversed whose radioresistant effect, indicating miR-340-5p is critical for hypoxic EV-induced radioresistance. KLF10 is the direct target of miR-340-5p. Moreover, metformin was found to increase the expression of KLF10 and enhance radiosensitivity of OSCC. And higher levels of miR-340-5p in the plasma exosomes of OSCC patients are related to poor radiotherapy response and prognosis.

Conclusions: Hypoxic tumour cell-derived exosomal miR-340-5p confers radioresistance in OSCC by targeting KLF10/UVRAG, suggesting that miR-340-5p could be a potential biomarker and therapeutic target for the enhancement of radiosensitivity in OSCC. Combined use of metformin and radiotherapy might benefit OSCC patients.

Background

Oesophageal cancer ranks sixth among cancer-associated deaths around the world. It has been reported that 572,034 oesophageal cancer diagnoses and 508,585 deaths occurred in 2018(1). In China, over 95% of oesophageal cancer patients are diagnosed with oesophageal squamous cell carcinoma (OSCC)(2). Most patients are diagnosed with locally advanced OSCC. For them, radiotherapy is an essential strategy(3). Despite radiotherapy advances, the prognosis of OSCC has been disappointing over the past 30 years: over 50% of patients have recurrence in 2 years, suggesting the significance of enhancing the radiosensitivity of OSCC(4–6).

Hypoxia is the critical cause of radioresistance: oxygen is a source of free radicals, which are needed for ionizing radiation (IR) to kill tumour cells; hypoxia can also induce a series of cellular biological transformations to escape the harmful effects of IR(7). When oxygen partial tension in the tumour microenvironment (TME) is below 0.13 kPa, radiobiological hypoxia that interferes radiation-induced cell death occurs(8). Thus, studies on the mechanism of hypoxia are essential to improve the efficacy of radiotherapy. Existing researches concerning hypoxia and radioresistance are mainly focused on hypoxic cells themselves, rather than the interactions between hypoxic cells and normoxic cells. The presence of hypoxic regions is typically distributed over the entire viable tumour mass. These hypoxic microregion are arranged on a micron level and exhibit sharp gradients between aerobic and hypoxic areas, and the two

intersected areas make short-distance intercellular communications very common(9). However, the communications between hypoxic cells and normoxic cells during radiation resistance remain unclear.

Exosomes and extracellular vesicles (EVs) are small particles of 30–200 nm in diameter that are encapsulated by dual membranes. EVs encapsulate various intercellular signal materials, including microRNA (miRNA)(10). Hypoxic tumour cells release specific EVs that can be endocytosed by adjacent cells in the TME, which subsequently causes a series of biological changes(11). The stable miRNAs capsulated by EVs can work as signal molecules to transmit hypoxia induced functional alterations such as resistance to therapy(12). The combination of hypoxia, EVs and TME may provide a novel insight into radiation resistance. However, data are still limited on this. In the current research, we revealed that hypoxic EVs can facilitate the growth and radioresistance of OSCC cells. We found that miR-340-5p is highly expressed in hypoxic OSCC EVs by high-throughput sequencing. miR-340-5p is directly transferred to normoxic OSCC cells and targets Kruppel-like factor 10 (KLF10), a tumour suppressor. Consequently, miR-340-5p blocks KLF10/UVRAG signaling and IR-induced apoptosis. Knockdown of miR-340-5p in hypoxic EVs can reverse these EV-induced oncogenic effects. Moreover, we demonstrated that the plasma exosomal miR-340-5p level can be used as a biomarker to predict in-field recurrence of OSCC patients, which provides a novel therapeutic target for OSCC patients.

Methods

3.1. Patients and specimens

All clinical samples were collected from the Department of Radiation Oncology, the First Affiliated Hospital of Nanjing Medical University. All subjects gave their informed consent before they participated in the study. The study was conducted in accordance with the Declaration of Helsinki, and the protocol was approved by the Ethics Committee and Institutional Review Board of the First Affiliated Hospital of Nanjing Medical University. A total of 88 OSCC patients were recruited in this study between 2017 and 2019. Clinical staging was based on the AJCC Cancer Staging Manual seventh edition(13). All patients underwent a 60 Gy total dose of involved-field radiation (2 Gy per fraction, 5 days per week) plus two cycles of concurrent chemotherapy of cisplatin and fluorouracil and two cycles of chemotherapy post-radiation. Radiation was delivered as described before(14). Blood samples were collected one day prior to definitive chemoradiation. Follow up studies included computed tomography, barium swallow, endoscopy and physical examination. All patients were followed up every 3 months until death or May 2020. In-field recurrence included primary lesion and involved regional lymph nodes inside PTV. Overall survival was defined as the interval between completion of radiation and death(14). We collected 30 ml whole blood from each patient using BD Vacutainer K2 EDTA Blood Collection Tubes (BD, USA), and we immediately centrifugated the whole blood at 4000 *g* for 10 min at 4 ℃ to get plasma. The plasma was then ultracentrifugated to collect EVs.

3.2. Cell culture and hypoxic treatment

Human OSCC cell lines (Te13, Te1 and Eca109) were obtained from American Type Culture Collection (ATCC, USA). All cell lines were cultured in RPMI-1640 medium (Gibco, USA) with 10% foetal bovine serum (FBS; Gibco, USA), 100 U/ ml penicillin and 100 μg/ml streptomycin. Cells were maintained at 37 °C and 5% CO_2 and were routinely examined for *Mycoplasma* contamination. To induce hypoxia (< 1% O_2), cells were cultured at 37℃ in the same incubator in an AnaeroPack jar with AneroPack-Anaero (Mitsubishi, Japan) according to the manufacturer's instructions. The hypoxic environment was confirmed by hypoxia inducible factor 1 subunit alpha (HIF-1α) expression. Cells were irradiated by an RS 2000 Pro X-Ray Bio-irradiator (Radsource, USA).

3.3. EV isolation and identification

FBS was depleted of EVs by ultracentrifugation at 140,000 *g* and 4 °C for 16 hours, and the supernatant was collected and filtered using a 0.22 μm filter (Millipore, USA). EVs derived from blood samples and cell medium were isolated by differential centrifugation as previously described(15). Before EV isolation, cells were cultured in normal medium until 50% confluency and then washed with phosphate-buffered saline (PBS) three times; and the medium was replaced with RPMI-1640 with 10% EV-depleted FBS and cultured under normoxic or hypoxic conditions. After 48 hours, the cell culture medium was harvested (50 ml), and EVs were isolated by differential centrifugation as previously described. The EVs were used immediately for further experiments. The size distribution and concentration of EVs were analysed by nanoparticle tracking analysis (NTA) using a ZetaView particle tracker from ParticleMetrix (Meerbusch, Germany). We used a transmission electron microscope (TEM; JEM-1200EX, JEOL Ltd., Japan) to observe the structure of EVs. CD63, CD81 and Alix were used as exosomal markers, and calnexin was used as a negative control for EVs. PKH67 (Sigma-Aldrich, USA) was used to label EVs. Twenty-four hours after PKH67-labelled EVs were incubated with OSCC cells, DAPI was used for nuclei staining. The cells were visualized with a confocal fluorescence microscope (Leica, Germany).

3.4. Western blotting

Samples of cells and EVs were washed and resuspended in RIPA lysis buffer (Beyotime, Shanghai, China) with a protease and phosphatase inhibitor mixture (Millipore). Proteins were separated based on their molecular weight by sodium dodecyl sulfate polyacrylamide gel electrophoresis and then transferred onto a polyvinylidene fluoride membranes (Millipore). The membranes were blocked with 5% skim milk powder in Tris-buffered saline containing Tween 20 (TBST) for 2 hours, and then the membranes were incubated at 4 °C overnight with specific primary antibodies (details are listed in Table S1). The membranes were rinsed in TBST for three times (10 minutes each time) and were incubated in secondary antibodies at room temperature for 2 hours and then were washed again in TBST (three times,10 minutes each time). Protein expression levels were detected by ECL Plus (Millipore) using a Bio-Imaging System (Bio-Rad, USA).

3.5. Quantitative real-time PCR (qRT-PCR)

Following the manufacturer's instructions, total RNA was extracted with TRIzol reagent (Invitrogen, USA). For qRT-PCR of mRNA, total RNA was further reverse transcribed into cDNA using the PrimeScript RT

reagent kit (Takara, Japan). For miRNA RT-PCR, we used the Mir-X miRNA First-Strand Synthesis Kit (Takara) to perform reverse transcription. The reactions were processed using a Real-time PCR System (Applied Biosystems 7500, USA) with a TB Green Premix Ex Taq Kit (Takara). The primers of target mRNA/miRNA were obtained from Wcgene Biotech (Shanghai, China). For normoxic cell samples, expression levels of genes and miRNAs were normalized to GAPDH or U6, respectively. Since hypoxia has an influence on the GAPDH expression, β-actin was obtained to evaluate gene levels in hypoxic cells(16). For EV samples, expression levels were normalized to external controls cel-miR-39 (RiboBio, Guangzhou, China). The results are shown in the form of relative expression calculated by the $2^{-\Delta\Delta CT}$ method.

3.6. Vector construction, lentivirus production and cell transfections

LV2-hsa-miR-340-5p-mimic vector and LV2-hsa-miR-340-5p-inhibitor vector were constructed as lentiviral vectors (GenePharma, Shanghai, China). Cells were infected when grown to 40–50% confluence and selected with puromycin for stable transfection. pcDNA3.1 vector containing ETS1, KLF10 and the negative control were purchased from GenePharma. siRNAs and mimics were purchased from RiboBio. Lipofectamine 3000 reagent (Invitrogen) was used for transfection. Sequences of vector were listed in Table S1.

3.7. 5-Ethynyl-2′-deoxyuridine (EdU) assay

We measured cell proliferation using an EdU assay kit (RiboBio). Twenty-four hours after coculture with EVs, cells were digested and seeded into 24-well plates (2×10^4 cells/well) and cultured with RPMI- 1640 (10% FBS) for 24 hours before adding EdU (50 μmol/L). According to the protocols, cells were then incubated for 2 hours at 37 °C, fixed in 4% paraformaldehyde for 30 minutes and permeabilized with 0.5% TritonX-100 for 10 minutes at room temperature. After washing with PBS, 1 × ApolloR reaction cocktail was added to react with the EdU for 30 minutes. Subsequently, Hoechst33342 was added for 30 minutes to visualize the nuclei. Images of cells were obtained under a Nikon microscope (Nikon, Japan). Proliferation was assessed using the mean number cells in three fields for each sample.

3.8. Luciferase report assay

Sequences corresponding to the 3′-UTR of KLF10 mRNA and containing the wild-type or mutated miR-340-5p binding sequence were synthesized by GeneScript (Nanjing, China). We inserted these sequences into the XbaI and SacI sites of the pmirGLO dual-luciferase miRNA target expression vector (Promega, USA). They were cotransfected with vectors and miR-340-5p-mimic/miR-340-5p-inhibitor or miR-NC by using a Lipofectamine 3000 (Invitrogen) according to the manufacturer's instructions. Luciferase activity was measured by Luciferase Reporter Assay System (Promega).

3.9. RNA immunoprecipitation (RIP)

The EZ-Magna RIP RNA Binding Protein Immunoprecipitation Kit (Millipore,) was used to conduct the RIP assay. Cells were collected and lysed by pre-cooled lysis buffer supplemented with 1 mM PMSF, protease inhibitor and RNase inhibitor. Cells were incubated with RIP buffer containing magnetic beads conjugated

with human anti-Argonaute 2 (Ago2) antibody (Millipore) or normal IgG (Millipore). Precipitate was digested and then co-immunoprecipitated RNA was isolated for PCR.

3.10. Colony formation assay

We seeded 200, 400, 800, 2000 and 5000 cells/well in 6-well plates one day before exposure to 0, 2, 4, 6 and 8 Gy irradiation, respectively. After two weeks, each well was washed with PBS for three times, then fixed with 4% paraformaldehyde for 30 minutes and finally stained with crystal violet. Colonies were counted with the naked eye. The survival curve was calculated using a single-hit, multi-target model.

3.11. Cell apoptosis analysis

Cell apoptosis was carried out using an apoptosis detection kit (Vanzyme, Nanjing, China) following the manufacturer's instructions. At 72 hours post-irradiation with 8 Gy, cells were digested and then resuspended in 500 μl of binding buffer with 5 μl of annexin V-FITC solution and 5 μl of propidium iodide (PI), and the cells were stained at room temperature for 15 minutes in the dark. Flow cytometry (FACScan; BD Biosciences, USA) and FlowJo software (BD, USA) were used to analyse the cells.

3.12. Immunofluorescence assay

A total of 5×10^4 cells were seeded into a confocal laser dish one day before 8 Gy irradiation. Four hours post-irradiation, cells were fixed in 4% paraformaldehyde at room temperature for 30 minutes and permeabilized in 0.1% Triton X-100 for 2 hours. Cells were then blocked with 5% BSA for 90 minutes and washed with PBS. After incubation with the primary antibody γ-H2AX (1:400; Cell Signalling Technology) overnight at 4°C, the cells were washed with PBS and incubated with an Alexa Fluor 555-conjugated secondary antibody (Beyotime) for 90 minutes. Cells were washed with PBS and treated with DAPI staining solution for 20 minutes and then observed using a confocal fluorescence microscope (Leica).

3.13. Tumour xenograft in nude mice model

This study was approved by the Institutional Animal Care and Use Committee of Nanjing Medical University (IACUC-1901012). BALB/c nude mice were purchased from the Animal Center of Nanjing Medical University. A total of 2×10^6 cells were injected subcutaneously into the flanks of nude mice. Tumours were measured by callipers every 5 days using the following formula: volume = $(\text{width}^2 \times \text{length})/2$. When the tumour volume reached 50 mm^3, 10 μg (50 μl) EVs or 50 μl PBS were injected into tumour once daily for 5 days. Meanwhile, tumours were irradiated by an RS 2000 Pro X-Ray Bio-irradiator (Radsource, USA) with 2 Gy per day for 4 consecutive days starting from the second day of EV injection. Two weeks post-IR, the mice were euthanized. In addition, we injected NC-Te13 cells and miR-340-5p mimics Te13 cells into the nude mouse flanks to study the effect of miR-340-5p. When the tumour volume reached 50 mm^3, four fractions of radiation (2 Gy/f) were applied to the tumours, and the mice were sacrificed 14 days after the radiation was completed. Lead shields were used to prevent radiation injury.

3.14. Immunohistochemistry

Immunohistochemistry was done as previously reported(17). Staining intensity was scored according to 4 grades: 0 (no staining), 1 (weak staining), 2 (intermediate staining), or 3 (strong staining). The staining percentages were divided into 4 grades: 0 (no positive), 1 (≤25% positive), 2 (25%-50% positive) and 3 (≥50% positive). The product of staining intensity and percentage was used as the final staining score.

3.15. TUNEL assay

The TUNEL assay was performed using the In Situ Cell Death Detection Kit (Roche, Germany). Following the manufacturer's protocols, sections were deparaffinized and rehydrated. Antigen retrieval was performed using hot 0.1 M citrate buffer pH 6.0, after which the sections were incubated with the TUNEL reaction mixture (containing TdT and fluorescein-conjugated dUTP) for 1 hour at 37℃. DAPI was used to stain nuclei. The apoptotic cells were analysed using a fluorescence microscope (Leica). For the negative control, TdT was not included in the reaction mixture.

3.16. Statistical analysis

All experiments in this study were carried out in triplicates. Differences between groups were determined using Student's t test, one-way ANOVA and two-way ANOVA. A chi-squared test was used to detect differences in clinical data. The patients were divided into high expression and low expression groups based on the median of gene expression. Kaplan-Meier analysis was used to compare recurrence in OSCC patients. Receiver operating characteristics (ROC) curves were constructed to evaluate the accuracy of prediction. STATA 14.0, SPSS 22.0 and GraphPad Prism 8.0 software were used to perform statistical analysis, and a p value < 0.05 was considered statistically significant (*p < 0.05, **p < 0.01, ***p < 0.001).

Results

4.1. Hypoxic tumour cell-derived EVs alleviate IR-induced apoptosis and promote radioresistance

EVs secreted by three OSCC cell lines were isolated by differential centrifugation. These EVs were clarified by methods as described before(18): NTA showed that the diameters of all three kinds of EVs were between 60–200 nm. TEM were used to observe the structures of EV. Exosomal markers Alix, CD63 and CD81 were highly detected in the EVs, while calnexin, an endoplasmic reticulum component, was absent in EV samples (Fig. S1A-C). To ensure the hypoxic environment, HIF1-α was used as a marker for the confirmation of hypoxia (Fig.S1D). EVs labelled by PKH67 were endocytosed by recipient cells (Fig.S1E). These data characterize EVs secreted by OSCC and indicate EVs derived from both normoxic and hypoxic OSCC cells can be endocytosed.

Next, we found EVs derived from OSCC cells under hypoxic environment contains higher levels of protein and RNA, indicating hypoxia may cause alterations of contents in EVs (Fig. 1A-B). In order to figure out the functions of EVs derived from the two different conditions, we cocultured OSCC cells with N-EV and H-EV, respectively. It was shown that H-EV, but not N-EV, drastically decreased the apoptosis in fed cells after IR (Fig. 1C-D). At the same time, the expression of DNA damage repair protein γ-H2AX was significantly declined in H-EV-fed cells after IR (Fig. 1E-F). To study the direct role of EVs in OSCC cells, we used GW4869, a widely used exosome secretion inhibitor, to reduce EV production. We found that GW4869 inhibited colony formation of OSCC cells after IR, but it had no effect on non-irradiated cells. Meanwhile, GW4869 only decreased the colony formation and increased apoptosis after IR of cells fed with H-EV (Fig.S2A-C). Also, the DNA damage caused by IR was alleviated in H-EV coculture cells detected by γ-H2AX as the concentration of H-EV rises. (Fig. 2G-H). Similarly, the apoptosis caused by IR and colony formation after IR showed the same results in H-EV fed cells in a dose-dependent manner (Fig. 1I, Fig.S2D). These results indicate that EVs secreted by hypoxic OSCC cells can promote radioresistance in normoxic cells.

We further verified the role of H-EV in radioresistance in tumour xenograft mice models (Fig. 1J). We found that injection of H-EV rather than N-EV or PBS drastically enhanced tumor growth only in IR group but not non-IR group (Fig. 1K-L). And the time for tumour xenograft to triple in size since the last day of IR was significantly shortened in irradiated H-EV group (Fig. 1M). Moreover, IR induced cell damage and apoptosis was shown as TUNEL positive cells, which was significantly reduced by H-EV supplement (Fig. 1N-O). These results confirm that hypoxic tumour cell-derived EVs can inhibit IR-induced apoptosis and promote radioresiatance.

4.2. miR-340-5p is highly expressed in H-EV and promotes radioresistance in OSCC

As important intercellular signal materials encapsulated by EV, we inferred that miRNAs may be associated with H-EV caused radioresistance in OSCC. We have previously reported high-throughput miRNA-seq in EVs derived from both normoxic and hypoxic conditions of OSCC cells and found that miR-340-5p in highly expressed in H-EV of OSCC (15). Former studies have reported that miR-340-5p plays a dual role in cancer development and progression. Also, there are researches that miR-340-5p is related to the invasion and migration function of OSCC. To further investigate the role of miR-340-5p in radiosensitivity, we transfected miR-340-5p mimic lentivirus into OSCC cells. qRT-PCR verified the transfection efficiency (Fig. 2A). Surprisingly, miR-340-5p mimics transfection drastically decreased apoptosis after IR (Fig. 2B). At the same time, we found miR-340-5p greatly reduced DNA damage after IR (Fig. 2C-D). According to previous studies, miR-340-5p is both an inhibitor of migration and invasion and a pro-cancer factor in proliferation (19, 20). While those results were focused only on in vitro results, we established tumour xenograft mice models to study the in vivo functions of miR-340-5p in OSCC. After transfection with miR-340-5p mimics lentivirus, the cells were subcutaneously injected to mice as aforementioned. Interestingly, we figured out that overexpression of miR-340-5p did not change the proliferation in non-IR groups but significantly promoted tumour growth after IR (Fig. 2E-F). Also. miR-

340-5p reduced apoptosis after IR as described by TUNEL assays (Fig. 2G-H). These results demonstrate that miR-340-5p decreases IR-induced apoptosis and DNA damage and promotes radioresistance in OSCC.

4.3. miR-340-5p is essential for hypoxic EV-induced radioresistance shift in OSCC

Having determined the direct function of miR-340-5p in OSCC radiosensitivity, we inferred that miR-340-5p is critical for H-EV-caused radioresistance transfer in OSCC. To study whether miR-340-5p is transferred as EV cargos, we cocultured OSCC cells with PBS, N-EV and H-EV, respectively. We found that miR-340-5p was largely elevated in H-EV but not N-EV fed cells compared to PBS-fed group (Fig. 3A). In order to rule out possible affections by free RNAs in the supernatants, we used RNase A to remove residual RNA contaminants in the supernatant of EV extracts, and the PCR results remained unchanged (Fig. 3B). Moreover, we used TritonX-100 and RNase A together to destroy RNA encapsulated by EV membrane and we found that this treatment reversed the effect of miR-340-5p escalation in H-EV fed cells (Fig. 3C). And the increase of miR-340-5p in H-EV recipient cells was in a time-dependent and dose-dependent manner (Fig. 3D-E). These results indicate that miR-340-5p is encapsulated in EVs and can be delivered from H-EV to the recipient OSCC cells.

To further investigate the function of miR-340-5p in H-EV-caused radioresistance, we knocked down miR-340-5p in OSCC cells (Fig. 3F). EVs secreted under hypoxic conditions by miR-340-5p knockdown cells (H-sh-miR-340-5p-EVs) and NC cells (H-NC-EVs) were extracted. q-PCR results showed that miR-340-5p expression did not change in cells fed with H-sh-miR-340-5p-EV (Fig. 3G). Next, we cocultured OSCC cells with H-NC-EVs and H-sh-miR-340-5p-EV, respectively. We found that uptake of H-sh-miR-340-5p-EV rescued the suppression of IR-induced apoptosis caused by H-EV (Fig. 3H- I). Also, it was shown that H-sh-miR-340-5p-EV lost the ability to reduce the expression of γ-H2AX in recipient cells (Fig. 3J). In vivo studies implied the same results that H-sh-miR-340-5p-EV reversed the TUNEL positive cell numbers in tumour xenografts after IR (Fig. 3K-L). In addition, injection of H-sh-miR-340-5p-EV in nude mice models did not produce the similar anti-radiation effect which was seen in H-EV group (Fig. 3M-N). Taken together, these results confirm that miR-340-5p is essential for hypoxic EV-induced radioresistance shift in OSCC.

4.4. miR-340-5p induces radioresistance by affecting KLF10/UVRAG axis

We employed bioinformatics of starBase (http://starbase.sysu.edu.cn/) (21) to investigate the downstream of miR-340-5p. The criteria for selection was at least 9 cancer types plus the intersection of the 4 predicted programs of microT, miRanda, PITA and TargetScan. We found KLF10 ranked first in the prediction list and an assumed acting site of KLF10-3'-UTR for miR-340-5p was detected (Fig. 4A). qRT-PCR and Western blot analyses revealed decreased KLF10 level in miR-340-5p overexpressed OSCC cells (Fig. 4B-C). Meanwhile, we found H-EV-fed cells exhibited lower KLF10 levels (Fig. 4D). IHC results implied that overexpression of miR-340-5p reduced the number of KLF10 positive cells in tumour xenograft mice

(Fig. 4E). We next carried out dual luciferase reporter assays to validate our assumption. Luciferase activity considerably decreased in cells expressing miR-340-5p mimics and wild type KLF10. On contrary, luciferase activity was elevated in cells expressing miR-340-5p inhibitor and wild type KLF10. However, luciferase activity did not drastically alter in the cells expressing miR-340-5p mimics/inhibitor and mutant KLF10 (Fig. 4I). In cells expressing miR-340-5p mimics, we found that KLF10 is upregulated, while in cells expressing miR-340-5p inhibitor, KLF10 was declined, as revealed by RIP results (Fig. 4J). These results prove that KLF10 is a direct target of miR-340-5p.

After determining KLF10 as a genuine downstream of miR-340-5p, we investigated the biological function of KLF10 in radioresistance of OSCC cells. First, we generated a KLF10 inhibitor lentivirus and transfected it into OSCC cells. The results from cytological experiments indicated that silencing KLF10 greatly reduced apoptosis of OSCC cell after IR (Fig. 5A). Knockdown of KLF10 protein also accelerated DNA damage repair after IR (Fig. 5B). UV radiation resistance-associated gene (UVRAG) has been widely recognized as a significant player in autophagy. Yet it is newly reported to be associated with chromosomal stability independent of autophagy. Previous studies have reported that KLF10 can transcriptionally suppressed UVRAG promoter activity, which subsequently affects the radio-sensitivity by modulating some key factors in apoptosis and DNA repair (22). In our study, miR-340-5p can directly target KLF10, we wonder whether miR-340-5p can modulate any key proteins in apoptosis and DNA damage repair in OSCC. We detected some key factors in apoptosis and DNA damage repair by immunoblot. As shown in Fig. 5C, silencing KLF10 decreased the expression of UVRAG, Bax and Bad but increased Bcl-2 expression in OSCC cells. Also, silencing KLF10 repressed γ-H2AX and p-DNApkcs. Collectively, we determined that KLF10 is a tumour suppressor and is crucial for IR-induced apoptosis and DNA damage repair. To further elucidate the role of KLF10 in miR-340-5p-mediated radioresistance, we transfected miR-340-5p mimic lentivirus and KLF10 mimic lentivirus together into OSCC cells. The rescue experiments confirmed that the radioresistance promoted by miR-340-5p overexpression can be counteracted by ectopic KLF10 expression (Fig. 5D-E). Besides, ectopic KLF10 expression rescued the miR-340-5p induced key protein change in apoptosis and DNA damage repair (Fig. 5F). Thus, these results indicate that miR-340-5p promotes growth and radioresistance by directly targeting KLF10/UVRAG axis.

4.5. Metformin increased KLF10 expression and enhanced radio-sensitivity of OSCC

Previous studies indicated that the incidence of metabolic diseases increased in KLF10 knockout mice and AMPK could phosphorylate KLF10(22). Metformin-induced activation of the energy-sensor AMPK is well documented. Since KLF10 depletion accounted for the radioresistance induced by H-EV, we tried to use metformin to upregulate KLF10. We firstly tested the effect of metformin treatment on IR induced apoptosis and DNA damage repair in vitro. We found that metformin drastically restored the decreased apoptosis and accelerated DNA damage repair after IR caused by coculture with H-EV (Fig. 6A-B). Next, we used immunoblotting assays to confirm whether metformin increased KLF10 expression regulated several key factors in irradiated OSCC cells fed with H-EV (Fig. 6C). Injection of H-EV and metformin

together in nude mice models reversed the radioresistant effect which was seen in H-EV group (Fig. 6D-E). In addition, in vivo studies implied the same results that metformin reversed the TUNEL positive cell numbers in tumour xenografts after IR in H-EV group (Fig. 6F). These results indicated that metformin reverses the decrease of KLF10 caused by H-EV supplement and can enhance radio-sensitivity in OSCC.

4.6. Upregulation of plasma exosomal miR-340-5p indicates radioresistance and correlates with poor response to radiotherapy in OSCC patients

Having determined that-EV can induce radioresistance of OSCC cells by transferring miR-340-5p, we wanted to evaluate its predictive value in radiotherapy response and survival after radiation in OSCC patients. We analysed histological miR-340-5p levels and plasma exosomal miR-340-5p levels in 88 OSCC patients receiving definitive chemoradiotherapy. Details of the patients' clinical characteristics are listed in Table S2. We identified that OSCC patients who had in-field recurrence within three years post-radiotherapy exhibited higher expression levels of both histological and plasma exosomal levels of miR-340-5p (Fig. 7A). High levels of both histological and plasma exosomal miR-340-5p are also associated with poorer in-field free survival and overall survival of OSCC patients, suggesting that miR-340-5p acts as a pro-cancer role in OSCC (Fig. 7B-C). In addition, in a prelimarnary study, we found that the expression of plasma exosomal miR-340-5p of OSCC patients can be used to predict the pathological complete remission (pCR) rate after receiving neoadjuvant therapy (Fig. 7D). However, the number of enrolled patients was quite small, more studies concerning this issue are needed in the future. Moreover, q-PCR analysis confirmed that the expression of KLF10 in OSCC tissue is negatively related to the level of both histological and plasma exosomal miR-340-5p in OSCC patients (Fig. 7E-G). IHC staining of OSCC biopsy further showed that the expression of KLF10 protein was highly raised in histologically miR-340-5p low expressed patients (Fig. 7H). Taken together, we conclude that miR-340-5p is a pro-cancer factor in OSCC and can be used as a biomarker to predict the prognosis of OSCC patients.

Discussion

Radiotherapy has been widely accepted as an essential treatment for cancers and is the first-line strategy for patients with locally advanced OSCC(23, 24). Unfortunately, radiation resistance is becoming increasingly severe and remains one of the major limitations in OSCC clinical therapy(25, 26). Therefore, investigating the molecular mechanisms underlying radioresistance may be of great significance for improving OSCC patient outcomes. Hypoxia is a critical cause of radioresistance(27). Although the radioresistance mechanisms of hypoxic cells themselves have been extensively studied, the complexity of the hypoxic response in the hypoxic TME needs to be defined more clearly.

EVs or exosomes are small membrane vesicles of 30–200 nm in diameter, which contains numerous signal molecules. Tumour-derived EVs may intermediate cellular communication, stimulating tumour proliferation and therapeutic resistance(28). In the hypoxic TME, depletion of oxygen and acid milieu can activate HIF-1α, which subsequently causes downstream protein changes in hypoxic cells. This leads to the large production of exosomes as well as alterations of exosomal nucleic acids profiles. EVs are

endocytosed by normoxic cells and the encapsulated nucleic acids are also transferred to normoxic cells. Consequently, a series of biological changes occur in normoxic cells(12). Many studies have demonstrated that exosomal miRNAs play important roles in cancer biology, with both diagnostic and therapeutic implications. miRNA can be horizontally transferred into normoxic cells through hypoxic EVs to modify the TME. A bystander effect caused by these transmitted hypoxic exosomal miRNAs can promote malignant transformations of normoxic cells(29).

In this study, we extracted EVs from OSCC cells in oxygen-depleted conditions by differential ultracentrifugation. In vivo and in vitro studies revealed accelerated proliferation and radioresistance of normoxic OSCC cells after incubation with hypoxic EVs, suggesting a cancer-promoting effect. Besides, we previously employed high-throughput sequencing techniques to identify the differentially expressed miRNAs in the H-EVs of Te13 cells, and we previously found that miR-340-5p was elevated in all three types of OSCC cell lines(15). miR-340-5p is known as both a tumour inhibitor and a tumour promoter in multiple cancers, including breast cancer(30), thyroid cancer(31), gastric cancer(32) and non-small cell lung cancer(33); According to previous studies, miR-340-5p is both an inhibitor of migration and invasion and a pro-cancer factor in proliferation in OSCC (19, 20). While these results were focused only on in vitro results, we established tumour xenograft mice models to study the in vivo functions of miR-340-5p in OSCC and we found that miR-340-5p promotes radioresistance. Moreover, miR-340-5p is critical for H-EV-casued radioresistancce shuttle in OSCC. To further investigate the mechanisms of miR-340-5p in OSCC, we employed bioinformatics to study its downstream. Out of these potential mRNA targets, KLF10 ranked first. The KLF family has been discovered to be occupied in essential cellular activities, including proliferation, differentiation, programmed cell death, and neovascularization (34); therefore, this family is involved in numerous aspects of tumourigenesis. In our research, we proved KLF10 is genuine target of miR-340-5p. Increased miR-340-5p in OSCC degrades KLF10 mRNA while KLF10 reversed the effects of the initiation of proliferation and inhibition of apoptosis caused by exosomal miR-340-5p both in vivo and in vitro.

KLF10 has been reported to transcriptionally suppressed UVRAG promoter activity, which subsequently affects the radio-sensitivity by modulating some key factors in apoptosis and DNA repair. A binding site resided in UVRAG promoter region was conformed to be inhibited by interacting with KLF10(22). In our research, we demonstrated that elevation of miR-340-5p and knockdown of KLF10 can decrease the expression of UVRAG, Bax and Bad but increase Bcl-2 expression in OSCC cells. Also, silencing KLF10 repressed γ-H2AX and p-DNApkcs. Metformin, a famous drug for diabetes, is reported to improve response to therapy and reprogram the tumour immune microenvironment in OSCC (35). Metformin can induce KLF10 expression via AMPK and increase radio-sensitivity of pancreatic cancer. In our study, we found that metformin can enhance radio-sensitivity by inducing KLF10 expression in H-EV-fed OSCC cells. Also, in vivo results confirmed its radio-sensitizing effect, which brings about its potential application in OSCC radiotherapy.

Having confirmed hypoxic EV and miR-340-5p are pro-cancer factors, we aimed to investigate its clinical value. We found that plasma exosomal miR-340-5p expression is positively associated with in-field

recurrence in OSCC. In addition, miR-340-5p levels in plasma EVs showed an encouraging accuracy in predicting radioresistance and prognosis. Liquid biopsy is currently used to monitor the response and predict prognosis in solid tumours. EVs containing miRNAs appear stable in plasma and are promising biomarkers for cancers(36). miRNAs contained in exosomes secreted by hypoxic tumour cells can reflect hypoxia in the entire TME. Compared with traditional hypoxic probe imaging, plasma exosomes reflect the effects of hypoxic microenvironment on cell biological functions, which may be a more important reason of radioresistance caused by hypoxia.

Conclusions

Our studies demonstrate that exosomes from hypoxic OSCC cells confer radioresistance by transferring miR-340-5p. miR-340-5p can block IR-induced apoptosis by negatively regulating KLF10 and UVRAG. Metformin can block the radioresistance shuttle by upregulating KLF10. Clinical specimens of OSCC demonstrated the predictive value of plasma exosomal miR-340-5p in radiation response, which provides novel insight into whether it is a potential biomarker and a therapeutic target for OSCC patients.

List Of Abbreviations

OSCC oesophageal squamous cell carcinoma

TME tumour microenvironment

EVs extracellular vesicles

IR ionizing radiation

KLF10Kruppel-like factor 10

PBS phosphate-buffered saline

TBST Tris-buffered saline containing Tween 20

qRT-PCR Quantitative real-time polymerase chain reaction

EdU 5-Ethynyl-2□-deoxyuridine

RIP RNA immunoprecipitation

ChIP Chromatin immunoprecipitation

CCK-8 Cell Counting Kit

ROC receiver operating characteristics

TEM transmission electron microscopy

NTA nanoparticle tracking analysis

H-EVs hypoxic extracellular vesicles

N-EVs normoxic extracellular vesicles

ETS1 ETS proto-oncogene 1

H-sh-miR-340-5p-EVs miR-340-5p knockdown hypoxic extracellular vesicles

H-NC-EVs hypoxic negative controll extracellular vesicles

UVRAG UV radiation resistance-associated gene

Declarations

Ethics approval and consent to participate

The study was conducted in accordance with the Declaration of Helsinki, and the protocol was approved by the Ethics Committee and Institutional Review Board of the First Affiliated Hospital of Nanjing Medical University. The animal experiment was approved by the Institutional Animal Care and Use Committee of Nanjing Medical University (IACUC-1901012).

Consent for publication

All the patients involved in our study obtained written consent for publication.

Availability of data and materials

The datasets used and/or analyzed during the current study are available upon request.

Competing interests

The authors declare that they have no competing interests.

Funding

This work was supported by the National Natural Science Foundation of China (No.81703024, No.81874217) and the Postgraduate Research & Practice Innovation Program of Jiangsu Province (KYCX18_1519).

Authors' contributions

FC, JL, XY, and XS contributed to the design of the study. FC, JG, JL and BX performed the experiments. FC, XY, and MT contributed to the writing and revision of the manuscript. All authors read and approved the final manuscript.

Acknowledge

We would like to thank the Core Facility of Jiangsu Provincial People's Hospital for its help in the detection of experimental samples and immunohistochemistry evaluations.

References

1. Bray F, Ferlay J, Soerjomataram I, Siegel RL, Torre LA, Jemal A. Global cancer statistics 2018: GLOBOCAN estimates of incidence and mortality worldwide for 36 cancers in 185 countries. CA Cancer J Clin. 2018;68(6):394–424.
2. Chen W, Zheng R, Baade PD, Zhang S, Zeng H, Bray F, et al. Cancer statistics in China, 2015. CA Cancer J Clin. 2016;66(2):115–32.
3. Lagergren J, Smyth E, Cunningham D, Lagergren P. Oesophageal cancer. Lancet. 2017;390(10110):2383–96.
4. Zeng H, Zheng R, Guo Y, Zhang S, Zou X, Wang N, et al. Cancer survival in China, 2003–2005: a population-based study. Int J Cancer. 2015;136(8):1921–30.
5. Gavin AT, Francisci S, Foschi R, Donnelly DW, Lemmens V, Brenner H, et al. Oesophageal cancer survival in Europe: a EUROCARE-4 study. Cancer Epidemiol. 2012;36(6):505–12.
6. Njei B, McCarty TR, Birk JW. Trends in esophageal cancer survival in United States adults from 1973 to 2009: A SEER database analysis. J Gastroenterol Hepatol. 2016;31(6):1141–6.
7. Horsman MR, Mortensen LS, Petersen JB, Busk M, Overgaard J. Imaging hypoxia to improve radiotherapy outcome. Nat Rev Clin Oncol. 2012;9(12):674–87.
8. Salem A, Asselin MC, Reymen B, Jackson A, Lambin P, West CML, et al. Targeting Hypoxia to Improve Non-Small Cell Lung Cancer Outcome. J Natl Cancer Inst. 2018;110(1).
9. Vaupel P, Mayer A. Tumor Oxygenation Status: Facts and Fallacies. Adv Exp Med Biol. 2017;977:91–9.
10. Yang X, Li Y, Zou L, Zhu Z. Role of Exosomes in Crosstalk Between Cancer-Associated Fibroblasts and Cancer Cells. Front Oncol. 2019;9:356.
11. Meng W, Hao Y, He C, Li L, Zhu G. Exosome-orchestrated hypoxic tumor microenvironment. Mol Cancer. 2019;18(1):57.
12. Shao C, Yang F, Miao S, Liu W, Wang C, Shu Y, et al. Role of hypoxia-induced exosomes in tumor biology. Mol Cancer. 2018;17(1):120.
13. Springer International Publishing
AJCC Cancer Staging Manual
Amin MB, Edge SB, Greene FL, Byrd DR, Brookland RK, Washington MK, et al. AJCC Cancer Staging Manual: Springer International Publishing; 2016.
14. Zhang X, Li M, Meng X, Kong L, Zhang Y, Wei G, et al. Involved-field irradiation in definitive chemoradiotherapy for locally advanced esophageal squamous cell carcinoma. Radiat Oncol.

2014;9:64.

15. Chen F, Chu L, Li J, Shi Y, Xu B, Gu J, et al. Hypoxia induced changes in miRNAs and their target mRNAs in extracellular vesicles of esophageal squamous cancer cells. Thorac Cancer. 2020;11(3):570–80.
16. Said HM, Katzer A, Flentje M, Vordermark D. Response of the plasma hypoxia marker osteopontin to in vitro hypoxia in human tumor cells. Radiother Oncol. 2005;76(2):200–5.
17. Zhang Z, Li J, Huang Y, Peng W, Qian W, Gu J, et al. Upregulated miR-1258 regulates cell cycle and inhibits cell proliferation by directly targeting E2F8 in CRC. Cell Prolif. 2018;51(6):e12505.
18. Thery C, Witwer KW, Aikawa E, Alcaraz MJ, Anderson JD, Andriantsitohaina R, et al. Minimal information for studies of extracellular vesicles 2018 (MISEV2018): a position statement of the International Society for Extracellular Vesicles and update of the MISEV2014 guidelines. J Extracell Vesicles. 2018;7(1):1535750.
19. Zhang Z, Liang X, Ren L, Zhang S, Li S, Wan T, et al. LINC00662 promotes cell viability and metastasis in esophageal squamous cell carcinoma by sponging miR-340-5p and upregulating HOXB2. Thorac Cancer. 2020.
20. Wang X, Gu M, Ju Y, Zhou J. PIK3C3 Acts as a Tumor Suppressor in Esophageal Squamous Cell Carcinoma and Was Regulated by MiR-340-5p. Med Sci Monit. 2020;26:e920642.
21. Li JH, Liu S, Zhou H, Qu LH, Yang JH. starBase v2.0: decoding miRNA-ceRNA, miRNA-ncRNA and protein-RNA interaction networks from large-scale CLIP-Seq data. Nucleic Acids Res. 2014;42(Database issue):D92-7.
22. Chang VH, Tsai YC, Tsai YL, Peng SL, Chen SL, Chang TM, et al. Krupple-like factor 10 regulates radio-sensitivity of pancreatic cancer via UV radiation resistance-associated gene. Radiother Oncol. 2017;122(3):476–84.
23. Xi M, Lin SH. Recent advances in intensity modulated radiotherapy and proton therapy for esophageal cancer. Expert Rev Anticancer Ther. 2017;17(7):635–46.
24. Kato H, Nakajima M. Treatments for esophageal cancer: a review. Gen Thorac Cardiovasc Surg. 2013;61(6):330–5.
25. van Hagen P, Hulshof MC, van Lanschot JJ, Steyerberg EW, van Berge Henegouwen MI, Wijnhoven BP, et al. Preoperative chemoradiotherapy for esophageal or junctional cancer. N Engl J Med. 2012;366(22):2074–84.
26. Sjoquist KM, Burmeister BH, Smithers BM, Zalcberg JR, Simes RJ, Barbour A, et al. Survival after neoadjuvant chemotherapy or chemoradiotherapy for resectable oesophageal carcinoma: an updated meta-analysis. Lancet Oncol. 2011;12(7):681–92.
27. Macedo-Silva C, Miranda-Goncalves V, Henrique R, Jeronimo C, Bravo I. The Critical Role of Hypoxic Microenvironment and Epigenetic Deregulation in Esophageal Cancer Radioresistance. Genes (Basel). 2019;10(11).
28. Mager SELA, Breakefield I, Wood XO. MJ. Extracellular vesicles: biology and emerging therapeutic opportunities. Nat Rev Drug Discov. 2013;12(5):347–57.

29. Melo SA, Sugimoto H, O'Connell JT, Kato N, Villanueva A, Vidal A, et al. Cancer exosomes perform cell-independent microRNA biogenesis and promote tumorigenesis. Cancer Cell. 2014;26(5):707–21.
30. Mohammadi Yeganeh S, Vasei M, Tavakoli R, Kia V, Paryan M. The effect of miR-340 over-expression on cell-cycle-related genes in triple-negative breast cancer cells. Eur J Cancer Care (Engl). 2017;26(6).
31. Zhao P, Ma W, Hu Z, Zhang Y, Zhang S, Wang Y. Up-regulation of miR-340-5p promotes progression of thyroid cancer by inhibiting BMP4. J Endocrinol Invest. 2018;41(10):1165–72.
32. Zhang L, Kang W, Lu X, Ma S, Dong L, Zou B. LncRNA CASC11 promoted gastric cancer cell proliferation, migration and invasion in vitro by regulating cell cycle pathway. Cell Cycle. 2018;17(15):1886–900.
33. Lu G, Zhang Y. MicroRNA-340-5p suppresses non-small cell lung cancer cell growth and metastasis by targeting ZNF503. Cell Mol Biol Lett. 2019;24:34.
34. Subramaniam M, Hawse JR, Johnsen SA, Spelsberg TC. Role of TIEG1 in biological processes and disease states. J Cell Biochem. 2007;102(3):539–48.
35. Wang S, Lin Y, Xiong X, Wang L, Guo Y, Chen Y, et al. Low-dose metformin reprograms the tumor immune microenvironment in human esophageal cancer: Results of a phase II clinical trial. Clin Cancer Res. 2020.
36. Siravegna G, Marsoni S, Siena S, Bardelli A. Integrating liquid biopsies into the management of cancer. Nat Rev Clin Oncol. 2017;14(9):531–48.

Figures

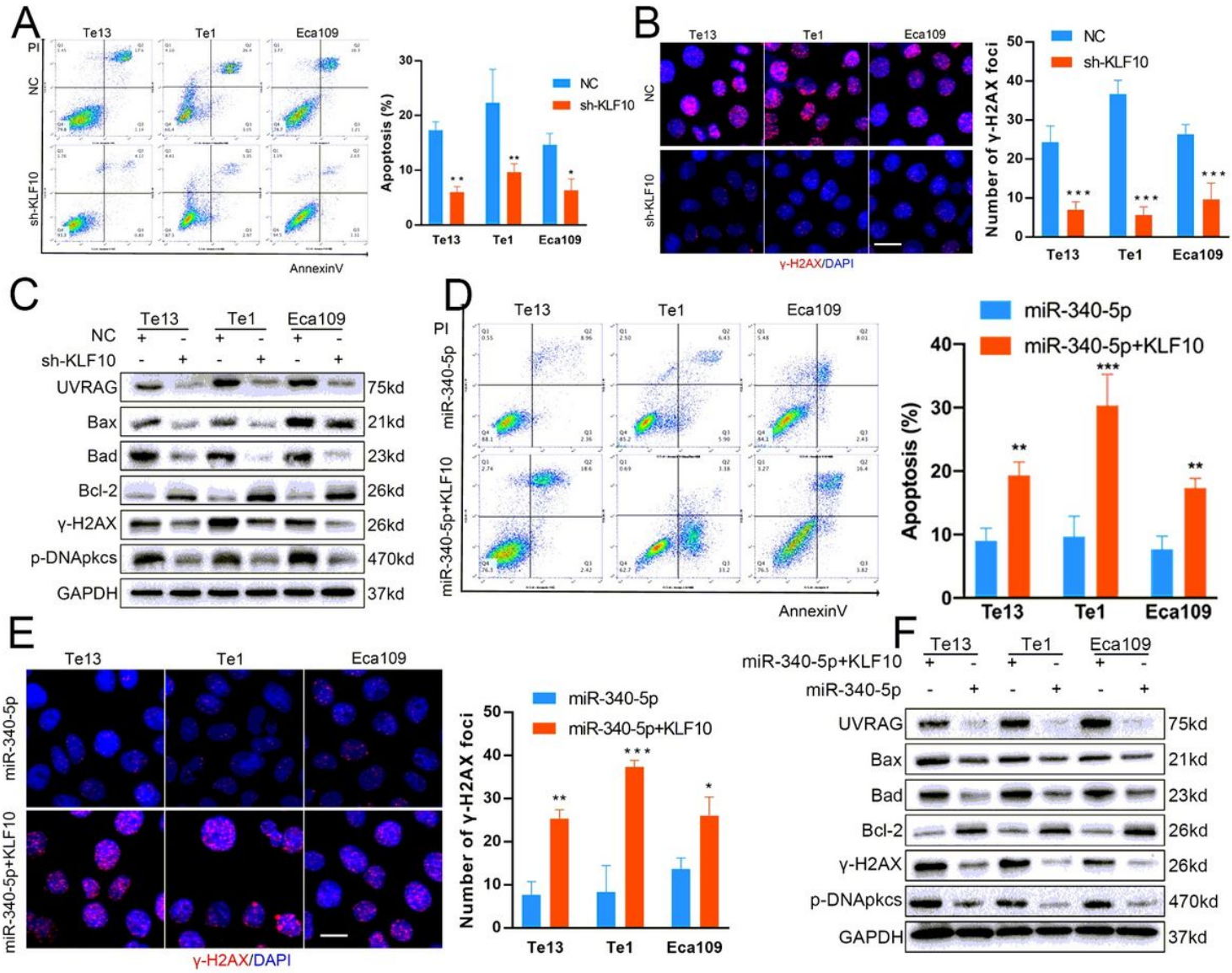

Figure 1

EVs derived from hypoxic OSCC cells promote radio-resistance. A-B EVs derived from OSCC cells under hypoxic environment contains more levels of protein (A) and RNA (B). C-D Coculture with H-EV drastically decrease apoptosis induced by irradiation of OSCC cells. E-F H-EV-fed OSCC cells expressed less DNA damage repair marker γ-H2AX after irradiation (scale bar=20μm). G-H The expression of γ-H2AX of irradiated OSCC cells was related to H-EV supplement in a dose-dependent manner (scale bar=20μm). I The apoptosis of OSCC cells caused by irradiation was decreased by H-EV coculture in a dose-dependent manner. J Schematic diagram of the experimental design used to establish the animal model. K Images of tumour in each group (n=6). L Alterations of tumour volume in each group (n=6). M Time to triple the tumour volume since the first EV injection day in each group (n=6). N-O H-EV-fed OSCC xenograft exhibited lower TUNEL positive cells after irradiation.

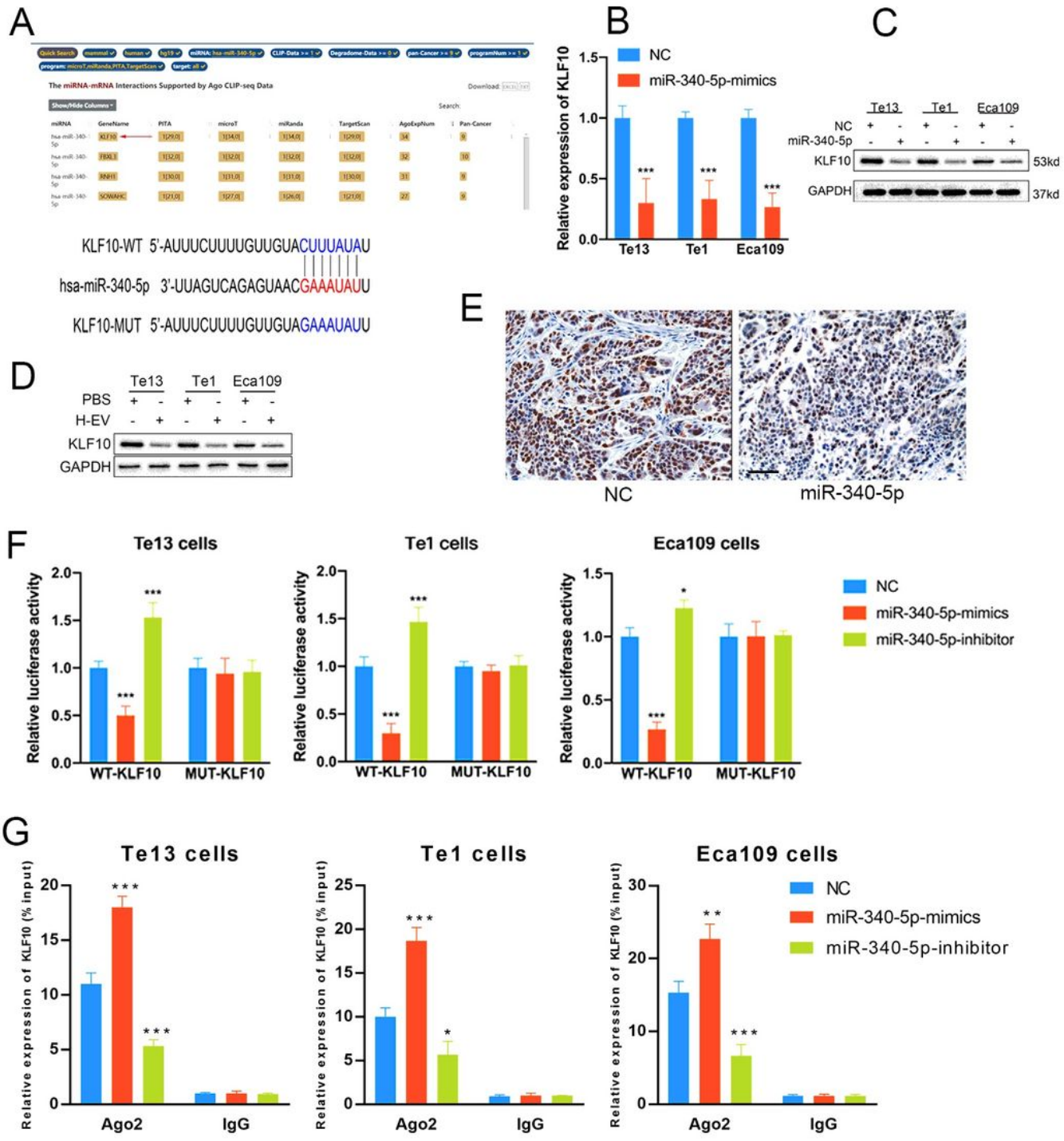

Figure 2

miR-340-5p promotes radioresistance in OSCC A qRT-PCR confirmed effect of miR-340-5p mimics transfection. B miR-340-5p overexpression suppressed irradiation caused apoptosis in OSCC cells. C The expression of γ-H2AX was decreased in miR-340-5p overexpressed OSCC cells after irradiation (scale bar=20μm). D Western blot assays demonstrated miR-340-5p blocked the expression of DNA damage repair protein γ-H2AX and p-DNApkcs after irradiation in OSCC cells. E Images of tumour in each group

(n=6). F Alterations of tumour volume in each group (n=6). G-H miR-340-5p overexpressed OSCC xenograft exhibited lower TUNEL positive cells after irradiation.

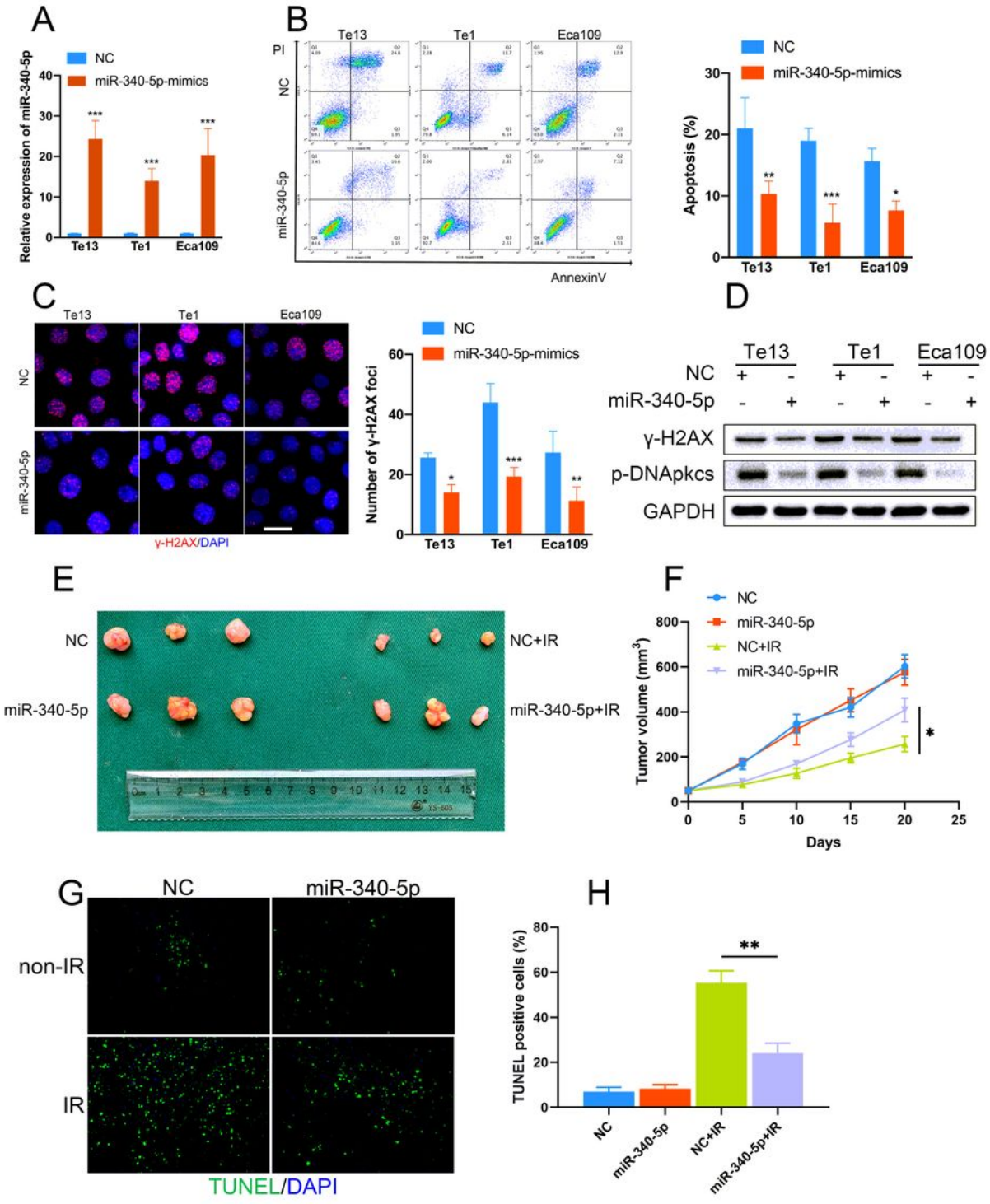

Figure 3

miR-340-5p is essential for hypoxic EV-induced radioresistance shift in OSCC A miR-340-5p was largely elevated in H-EV but not N-EV fed OSCC cells. B qRT-PCR revealed miR-340-5p expression of OSCC cells after coculture with RNase A treated EV. C miR-340-5p levels in OSCC cells fed with RNase A or RNAase A

and TritonX-100 together as detected by qRT-PCR assays. D-E The expression of miR-340-5p in OSCC cells was associated with H-EV supplement in a time-dependent (D) and dose-dependent (E) manner. F qRT-PCR confirmed effect of miR-340-5p knockdown in OSCC cells. G No significant changes were observed by qRT-PCR between OSCC cells cocultured with PBS or H-sh-miR-340-5p-EV. H-I Knockdown of miR-340-5p in hypoxic EVs rescued the suppression of IR-induced apoptosis caused by H-EV. J Knockdown of miR-340-5p in hypoxic EVs reversed decrease of γ-H2AX after irradiation in OSCC cells caused by H-EV supplement (scale bar=20μm). K-L Knockdown of miR-340-5p in hypoxic EVs recused TUNEL positive cell numbers in OSCC xenografts after irradiation. M Alterations of tumour volume in each group (n=6). N Images of tumour in each group (n=6).

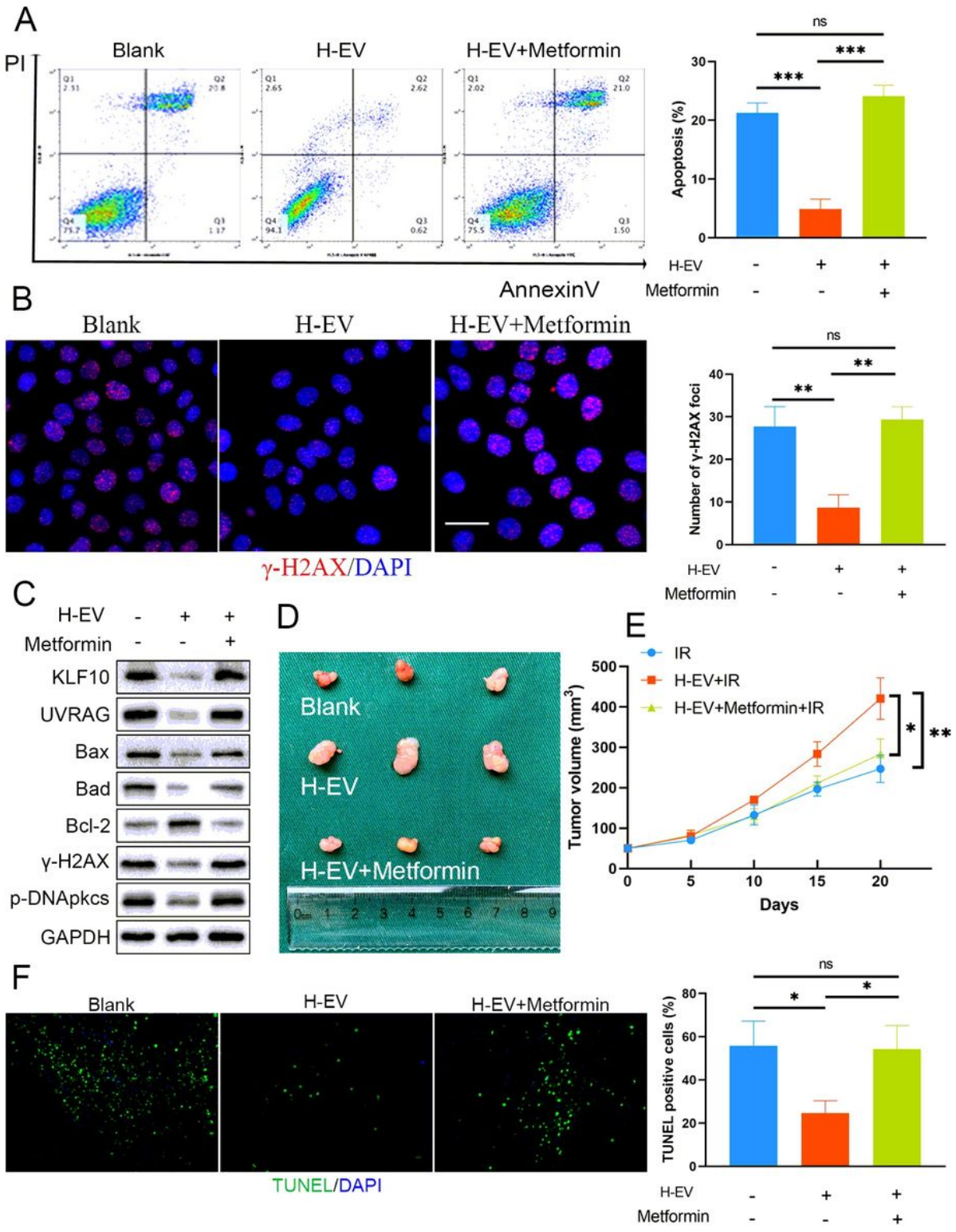

Figure 4

KLF10 is a direct target for miR-340-5p A Illustration of the putative predicted miR-340-5p binding site in the KLF10 mRNA 3'-UTR region. B-C Expression of KLF10 in OSCC cells transfected with relevant lentivirus was detected by qRT-PCR (B) and western blot (C). D Expression of KLF10 in OSCC cells were decreased after cocultured with hypoxic EVs. E Expression of KLF10 was detected by IHC in xenograft transfected with relevant lentivirus (scale bar=200μm). F Luciferase reporter assays were conducted to

verify that miR-340-5p bind to the 3'-UTR region of KLF10 directly. G RIP assays confirmed the binding status between miR-340-5p and KLF10 in treated and untreated OSCC cells, respectively.

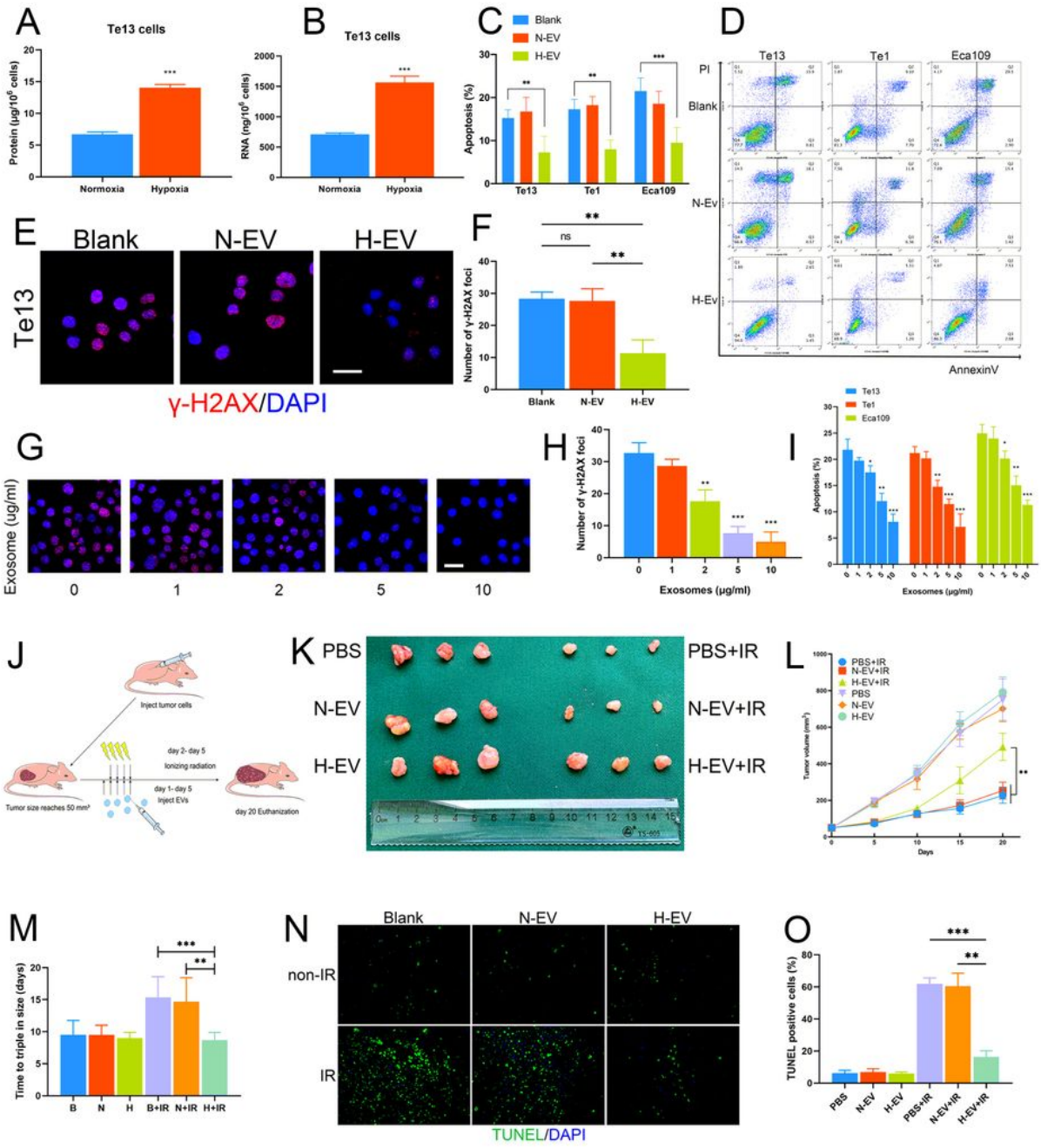

Figure 5

miR-340-5p induces radioresistance by affecting KLF10 A KLF10 knockdown attenuated apoptosis caused by irradiation in OSCC cells. B KLF10 knockdown decreased expression of DNA damage repair protein γ-H2AX (scale bar=20μm). C Western blot detected several key factors in apoptosis and DNA

damage repair. D-F Overexpression of KLF10 in miR-340-5p mimics lentivirus transfected OSCC cells rescued the apoptosis (D), DNA damage repair (E, scale bar=20μm), and several key proteins after irradiation (F).

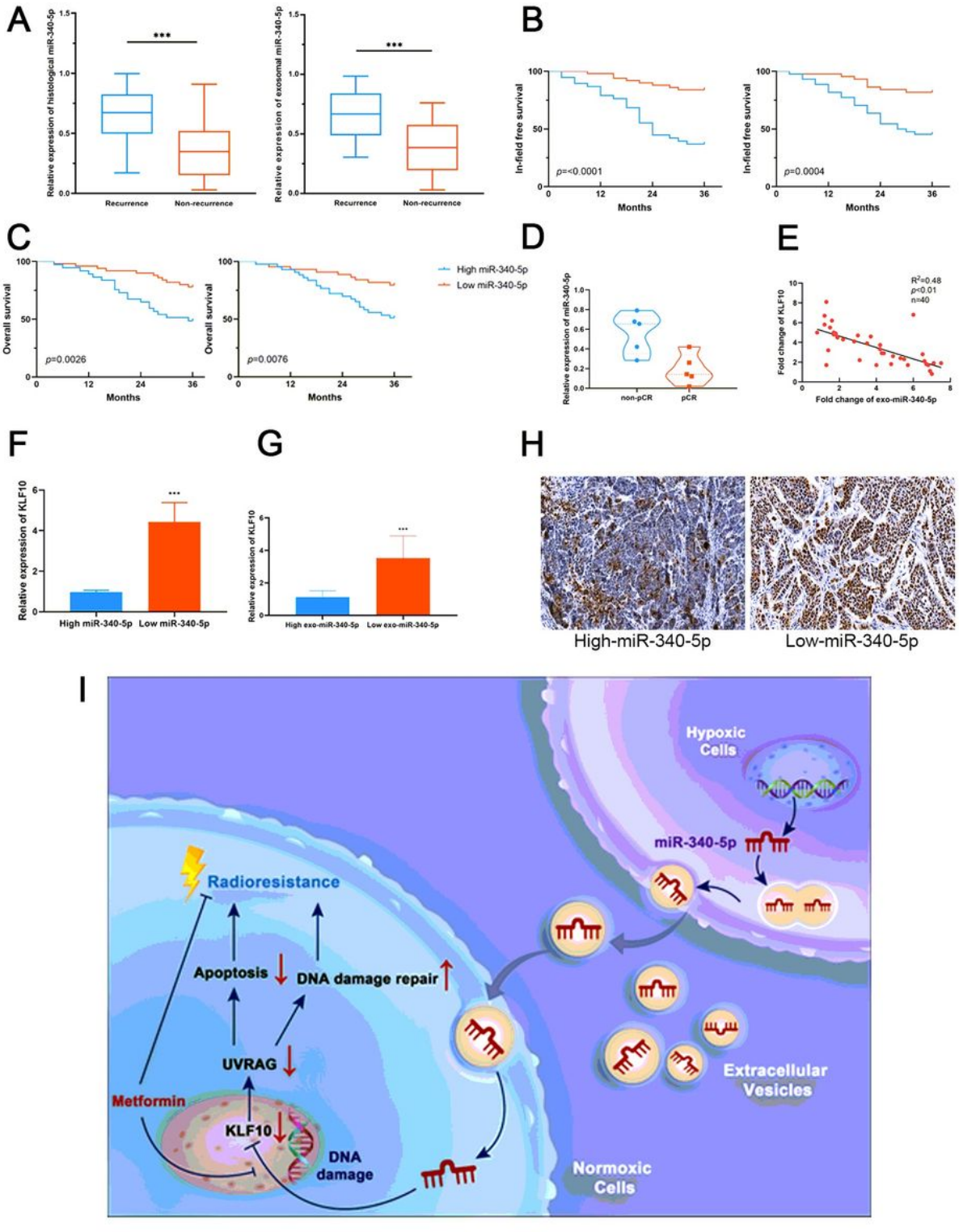

Figure 6

Metformin increased KLF10 expression and enhanced radio-sensitivity of OSCC A-B Metformin restored the decreased apoptosis (A) and accelerated DNA damage repair (B, scale bar=20μm) after irradiation

caused by coculture with H-EV. C Metformin increased KLF10 expression regulated several key factors in irradiated OSCC cells fed with H-EV. D Images of tumour in each group (n=6). E Alterations of tumour volume in each group (n=6). F TUNEL positive cell numbers were downregulated after metformin supplement.

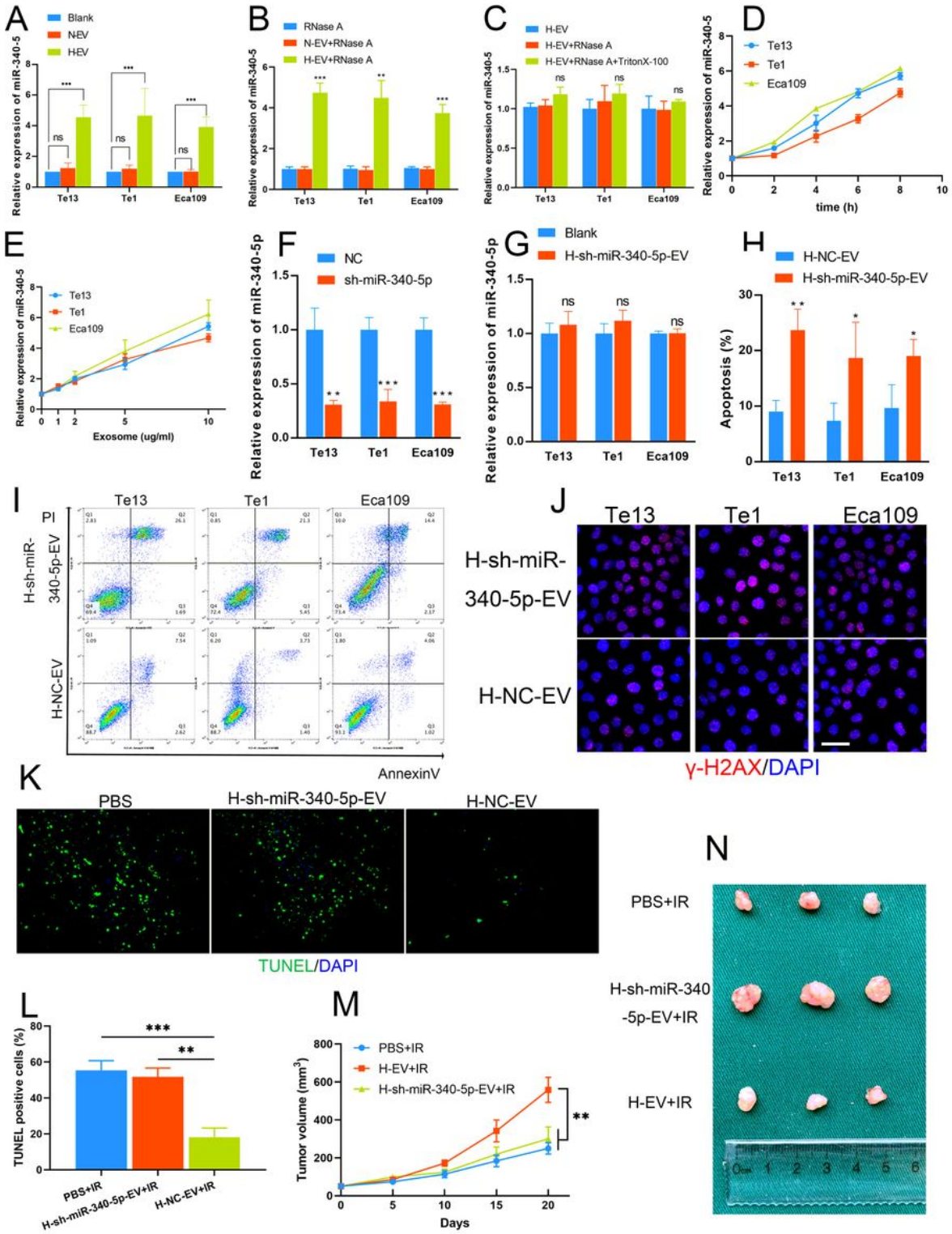

Figure 7

Upregulation of miR-340-5p indicates radioresistance and correlates with poor response to radiotherapy in OSCC patients A qRT-PCR analysis of miR-340-5p in tissues and plasma exosomes of OSCC patients with in-field recurrence and non-recurrence within 3 years post-radiotherapy. B-C Kaplan-Meier survival curve analysis of in-field free survival (B) and overall survival (C) of OSCC patients with different histological and plasma exosomal miR-340-5p levels in 3 years post-radiotherapy. D Expression of plasma exosomal miR-340-5p in 10 OSCC patients receiving neoadjuvant chemoradiotherapy. E Expression of KLF10 was negatively correlated with plasma exosomal miR-340-5p in 40 OSCC patients. F-G Expression of KLF10 was detected by qRT-PCR in clinical samples of patients with different miR-340-5p in OSCC tissues (F) and plasma EVs (G). H IHC showing the expression of KLF10 in clinical specimens expressing different miR-340-5p levels. I Schematic diagram showing that metformin attenuates hypoxic tumour cell-orchestrated radioresistant cascades.

Supplementary Files

This is a list of supplementary files associated with this preprint. Click to download.

- Figurelegends.docx
- TableS2ClinicalFeatures.docx
- TableS1AntibodiesandVectorSequences.xlsx
- S2.tif
- S1.tif